An additive manufactured CubeSat mirror incorporating a novel circular lattice

Robert Snell, Carolyn Atkins, Hermine Schnetler, Iain Todd, Everth Hernández-Nava, Alistair R. Lyle, George Maddison, Katherine Morris, Christopher Miller, Mélanie Roulet, Emmanuel Hugot, Fabio Tenegi Sanginés, Afrodisio Vega-Moreno, L. T. G. (Bart) van de Vorst, Joris Dufils, Leon Brouwers, Szigfrid Farkas, György Mező, Mat Beardsley, and Michael Harris

Published version information:

Citation: RM Snell et al. "An additive manufactured CubeSat mirror incorporating a novel circular lattice." Proceedings of SPIE, vol. 11451 (2020): 114510C. Is in proceedings of: **SPIE Astronomical Telescopes + Instrumentation 2020**, Online Only, United States, 14-18 Dec 2020.

DOI: 10.1117/12.2562738

PROCEEDINGS OF SPIE

SPIEDigitalLibrary.org/conference-proceedings-of-spie

An additive manufactured CubeSat mirror incorporating a novel circular lattice

Snell, Robert, Atkins, Carolyn, Schnetler, Hermine, Todd, Iain, Hernández-Nava, Everth, et al.

Robert Snell, Carolyn Atkins, Hermine Schnetler, Iain Todd, Everth Hernández-Nava, Alistair R. Lyle, George Maddison, Katherine Morris, Christopher Miller, Mélanie Roulet, Emmanuel Hugot, Fabio Tenegi Sanginés, Afrodisio Vega-Moreno, L. T. G. (Bart) van de Vorst, Joris Dufils, Leon Brouwers, Szigfrid Farkas, György Mező, Mat Beardsley, Michael Harris, "An additive manufactured CubeSat mirror incorporating a novel circular lattice," Proc. SPIE 11451, Advances in Optical and Mechanical Technologies for Telescopes and Instrumentation IV, 114510C (13 December 2020); doi: 10.1117/12.2562738

SPIE.

Event: SPIE Astronomical Telescopes + Instrumentation, 2020, Online Only

An additive manufactured CubeSat mirror incorporating a novel circular lattice

Robert Snell[a], Carolyn Atkins[b], Hermine Schnetler[b], Iain Todd[a], Everth Hernández-Nava[a], Alistair R. Lyle[a], George Maddison[a], Katherine Morris[b], Christopher Miller[b], Mélanie Roulet[c], Emmanuel Hugot[c], Fabio Tenegi-Sanginés[d], Afrodisio Vega-Moreno[d], L.T.G. (Bart) van de Vorst[e], Joris Dufils[e], Leon Brouwers[e], Szigfrid Farkas[f], György Mező[f], Mat Beardsley[g], and Michael Harris[g]

[a]Dept of Materials Science and Engineering, University of Sheffield, Sheffield, S1 3JD, UK
[b]UK Astronomy Technology Centre, Royal Observatory, Edinburgh, EH9 3HJ, UK
[c]Aix Marseille Univ, CNRS, CNES, LAM, Marseille, France
[d]SOLLIANCE / TNO, High Tech Campus 21, NL-5656 AE Eindhoven, The Netherlands
[e]Konkoly Observatory, Research Centre for Astronomy and Earth Sciences, MTA Centre for Excellence, 1121 Konkoly-Thege Miklós út 15-17, Budapest, Hungary
[f]Instituto de Astrofísica de Canarias (IAC), 38200, La Laguna, Tenerife, Spain
[g]RAL Space, Harwell Science & Innovation Campus, OX11 0QX, UK

ABSTRACT

Additive Manufacturing (AM; 3D printing) for mirror fabrication allows for intricate designs that can combine lightweight structures and integrated mounting. Conventional lightweight structures utilise cubic or prismatic unit cells, which do not provide uniform support at the edge of curved mirrors. We present a new circular lattice based upon cylindrical coordinates and how this lattice has been incorporated within an 80 mm diameter mirror intended for use in a 3 U CubeSat telescope. Several design iterations are explored, which include prototype mirrors produced in a titanium alloy and a finite element analysis of the one of the design iterations.

Keywords: Additive manufacturing, 3D printing, lightweight mirrors, metal mirrors, CubeSat, finite element analysis, lightweight structures, lattice

1. INTRODUCTION

Additive manufacture (AM; 3D printing) is a fabrication method which creates an object *layer-upon-layer* from a digital design file. Recent advances in AM now allow the realisation of functional components, in addition to its early adoption for prototyping. The primary advantage of AM is the freedom of design, which promotes the use of structures that would not be possible, or practical, via subtractive, formative or fabricative manufacturing methods. Aerospace and medical industries have led the way with the inclusion of AM within their production chains; however, uptake within the astronomical community has been slow. In 2017, a multi-institutional European team commenced collaboration on A2IM (Additive Astronomy Integrated-Component Manufacturing), a work package within the larger OPTICON framework (Optical Infrared Coordination Network for Astronomy) and funded by the European Commission Horizon 2020 programme. An overview of the A2IM work package is presented at this conference by *Schnetler et al. (2020)*,[1] with further A2IM prototype contributions discussed in papers by *Farkas et al. (2020)*,[2] *Vega et al. (2020)*[3] and *Roulet et al. (2020)*.[4] This paper presents an A2IM prototype development towards lightweight mirror technology for nano-satellite applications.

The primary benefit of AM for lightweight mirror development is the increase in design freedom, which removes some of the geometry restrictions imposed by conventional manufacturing methods. The increase in design freedom enables more function-optimised lightweight structures and part consolidation (where the mirror

Further author information:
e-mail: r.m.snell@sheffield.ac.uk

Advances in Optical and Mechanical Technologies for Telescopes and Instrumentation IV, edited by Ramón Navarro, Roland Geyl, Proc. of SPIE Vol. 11451, 114510C
 · doi: 10.1117/12.2562738

and mount can be combined into a single component). Several international teams have demonstrated the potential of AM substrates to be used directly as a mirror surface either after polishing or diamond turning,[5–9] or, indirectly as a core substrate prior to coating with nickel phosphorous (NiP).[10–12] Directly polished or diamond turned AM substrates in aluminium (AlSi10Mg) have demonstrated a surface roughness (root mean square, RMS) between 7.5 nm to 22 nm[5,6] for polishing, and 3 nm to 8 nm[8,9] for diamond turning, leading to suitability for near infrared applications. In addition, innovative AM specific lightweight structures are under investigation, for example: organic cellular structures (Voronoi cells) have been successfully demonstrated for a lightweight mirror core;[11,12] the use of topology optimisation (TO) has been implemented,[5,7] where a given volume is optimised following given constraints on mass and applied force; and further, several teams have investigated theoretically combining organic structures and TO for mirror design.[13–16] However, harnessing the benefits of AM and simultaneously ensuring that the design can be optically fabricated is challenging; although AM increases the design freedom there are limitations and a AM built geometry does not necessarily interface suitably with the conventional machining techniques to convert the AM substrate into a functional mirror.

This paper will describe the evolution of an innovative conformal circular lattice structure made possible via AM and the process of ensuring that the design can be processed to create the mirror surface. It is the process-chain of *design* → *manufacture* that is the primary objective of the study, as opposed to the optical quality that can be achieved. The mirror dimensional requirements are based upon a nano-satellite (nanosat; CubeSat) payload structure designed for Earth observation (EO) and builds upon previous AM mirror development for CubeSats.[17,18] This paper will present the mirror requirements (mechanical and optical) for the design (Section 2), the first iteration of the mirror design incorporating a novel circular lattice (Sections 3 and 4), subsequent iterations of the design to ensure compliance with build guidelines (Section 5), analysis using a finite element model (Section 6) and concluding with a summary and and description of future work (Section 7).

2. DESIGN REQUIREMENTS

2.1 Design inspiration

The A2IM prototype design requirements build upon a previous study presented in *Atkins et al. (2019a)*.[17] In the study, five AM metal mirrors were manufactured via polishing or diamond turning in a variety of materials for integration within a 3 U CubeSat chassis. The objective of the study was to investigate the quality of the mirror surface after post-processing, rather than reducing the mass of the mirror or part consolidation. Figure 1 highlights one of the polished AM mirrors and a cross-section demonstrating the lightweight design - a thorough description of the internal design is provided in *Atkins et al. (2019b)*.[18] The mirror dimensions were 84 mm diameter, 17.3 mm in height and with a spherical concave optical prescription of 350 mm radius of curvature. To reduce weight, a body centred cubic (BCC) lattice was used within the internal cavity, which reduced the weight to ∼ 69% of a solid equivalent.

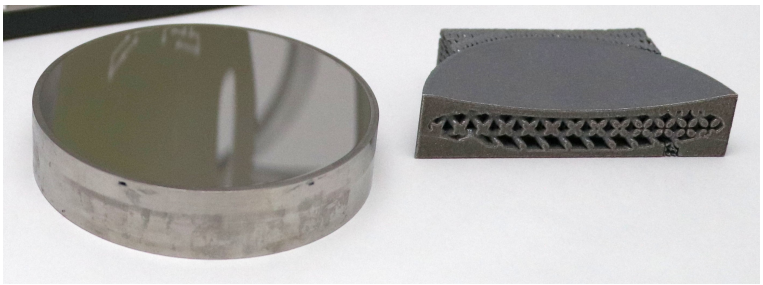

Figure 1. *Left* - the polished AM titanium alloy (Ti-6Al-4V) mirror; *right* - a cross-section through the raw aluminium alloy (AlSi10Mg) AM substrate highlighting the cavity populated with the BCC lattice. Image credit: NSTP3-PF2-008 Team.

2.2 A2IM CubeSat mirror prototype design concept

The objective of the A2IM CubeSat mirror design is to focus on the design benefits of AM and to ensure that these benefits can be realised at each step of the mirror fabrication process chain. In the previous study,[18] the

AM design was constrained to facilitate the generation of the optical surface, rather than harnessing the full benefit of the design freedom. Therefore this study investigates specifically the adoption of the benefits of the AM design space for mirror fabrication - i.e. innovative *lightweight structures* and *integrated mounting* - while easing the optical requirements to aid machining in the first instance. Figure 2 depicts the generic AM mirror process chain and highlights the additional processing steps that are required through the use of AM.

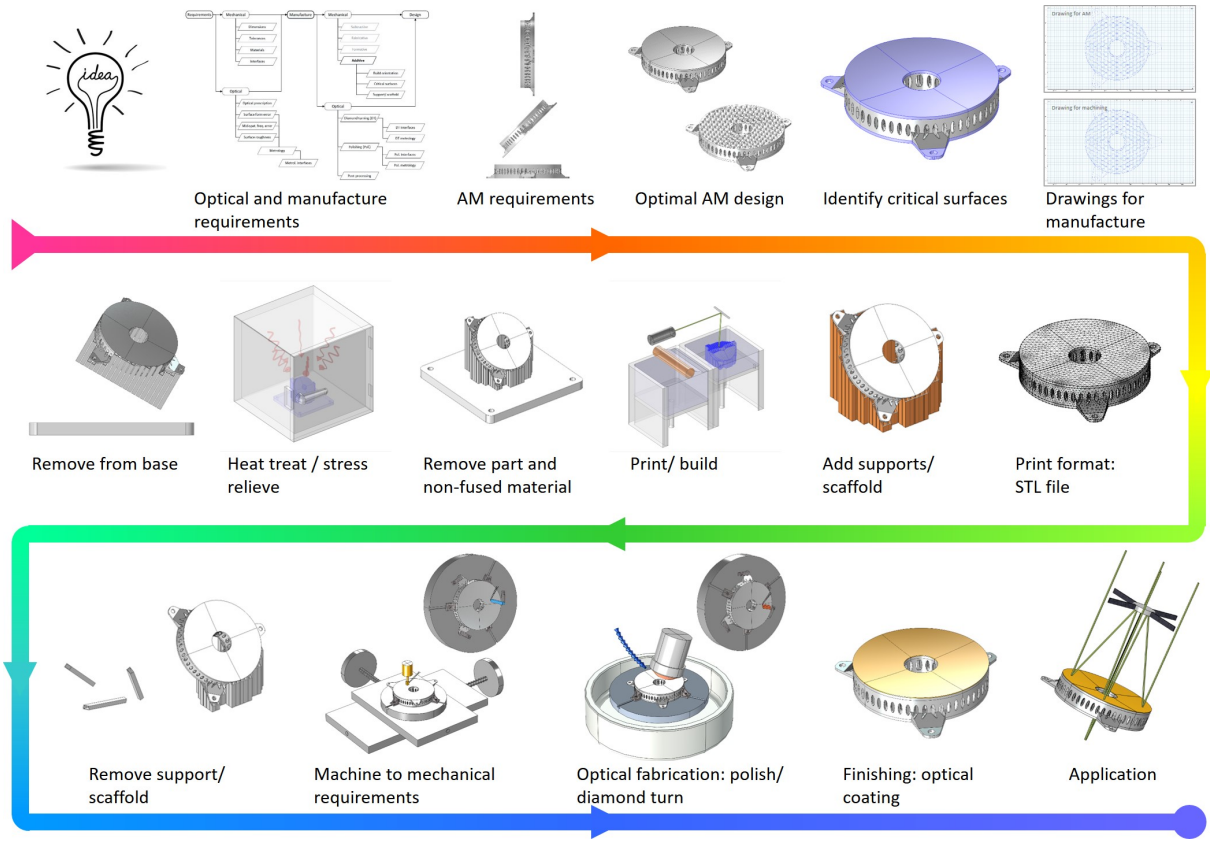

Figure 2. The generic AM mirror process chain starting with an *Idea* (*top-left*) and ending with the *Application* (*bottom-right*).

2.2.1 Mass reduction - lightweight structures

The mirror presented in Figure 1 was $\sim 69\%$ the mass of an equivalent solid - i.e. $\sim 31\%$ of the material has been removed. The objective for the A2IM prototype is to reduce the mass further to between 30% and 40% the mass of an equivalent solid. A mass reduction of this magnitude would be equivalent to lightweight mirrors created via material subtraction (*open-back mirrors*) or via fabricative methods (*sandwich mirrors*).[19]

In parallel to the fabrication of the mirrors in the previous study, an optimisation investigation was undertaken to explore how the mass of the mirror design could be decreased (w.r.t. the original 69% mass reduction) without negatively impacting the structural performance of the mirror.[18] The investigation suggested that the mass could be reduced to $< 50\%$ mass remaining without detrimentally impacting the print-through effect (*quilting*) of the lightweight structure upon the mirror surface. A variety of mass reduction routes were investigated: topology optimisation; lattice generation via AM design software; and structures inspired by nature. In addition, an early trial of a conformal lattice was explored that mapped a replicating lattice unit cell within a cylindrical geometry. However, one question that the investigation into did not answer was whether the designs could be printed.

2.2.2 Part consolidation - integrated mounting

Part consolidation is the combining of multiple individual components into a single object without the need for interfaces or fixtures. For the case of a mirror this could include combining a mirror with a mounting

interface, or integrating cooling channels. There are clear benefits for part consolidation, for example, having material continuity, or reducing the part count. Figure 3 highlights from the previous study[17] how the mirror and mount were fabricated as two parts and then combined to attach the mirror to the CubeSat chassis. Using this example, part consolidation of five components (mirror, mount and screws) can be combined as a single part with a nominally homogeneous material.

Figure 3. An example of how the mirror from the previous CubeSat study has been integrated within a 3 U CubeSat chassis using a mount - by implementing part consolidation, the mirror and mount could be a single component. Image credit: NSTP3-PF2-008 Team.

2.3 A2IM CubeSat mirror prototype design requirements

Table 1 provides a summary of the design requirements for the A2IM prototype mirror. The geometric requirements represent the bounding volume of the CubeSat chassis. The mechanical dimensions originate from the paper study *CubeSat Camera (CCAM)*,[20] which provided a description of a 3 U EO satellite utilising a 1.2 U Cassegrain telescope. The A2IM prototype uses a simplified optical prescription to facilitate the optical fabrication and evaluation. The selection of aluminium as the substrate material draws on previous experience in using AM aluminium and successful results obtained via single point diamond turning (SPDT).[7,17] The quality of the optical surface is not a priority of the prototype and an iterative approach to SPDT will not be employed to obtain a given optical performance as the objective of the prototype is to ensure that an innovative AM design can be processed; however, the prototype will aim for a surface roughness of <5 nm RMS. Figure 4 presents the initial concept design for the A2IM prototype mirror based upon the specifications described in Table 1.

Table 1. A2IM prototype mirror design requirements

Property	Value
Optical prescription, geometry	Flat, annulus
Outer diameter	83 mm⌀
Inner diameter	32 mm⌀
Mirror surface thickness	1.5 mm
Height	10 mm to 20 mm
Material	Aluminium alloy
Optical fabrication	SPDT
Mass reduction	30% to 40% of an equivalent solid
Mirror mount	Integrated with mirror
Mounting	To interface with a 3 U CubeSat chassis
Surface roughness	<5 nm RMS

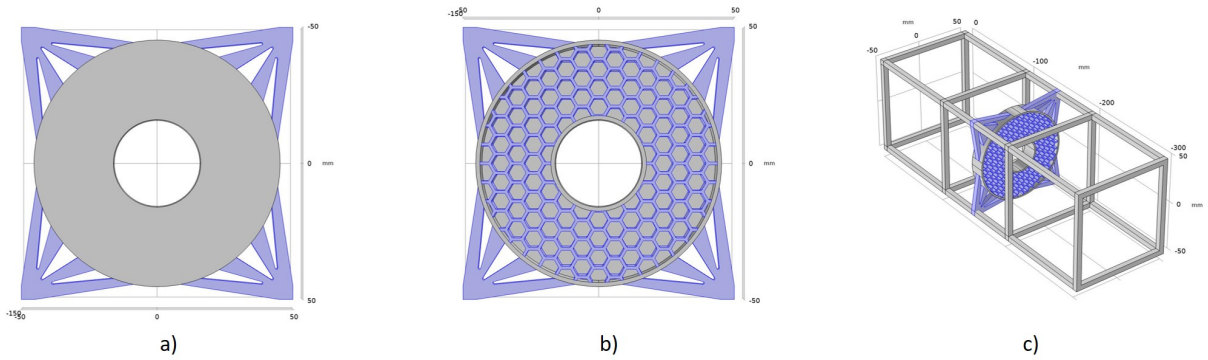

Figure 4. An initial concept of the A2IM CubeSat mirror prototype: *a)* - the mirror surface (grey) and integrated mounting (blue); *b)* the backside of the mirror highlighting a lightweight structure; and *c)* the prototype integrated within the CubeSat chassis.

3. UNIT CELL DESIGN

3.1 Mirror body

Conventional lightweight mirrors (open-back and sandwich variants) rely on lightweight structures composed of tessellating 'pockets' (unit cells) in the shape of cuboids,[21] triangular[22] prisms, or hexagonal[23] prisms. These structures provide a uniform support at the centre of the mirror, but fitting these unit cells uniformly at the edge of a circular or ellipsoidal mirror is problematic, leading to either fractions of unit cells being used (*Hubble Space Telescope*[21]), or an alteration of unit cell geometry (Giant Magellan Telescope[23]). The same problem is exhibited by replicating lattice structures, a geometry style frequently used in AM, but only now being explored for mirror fabrication.

There are potential solutions to this problem. Lattices can be made 'conformal', so that lattices are distorted to fit the perimeter of a volume. However, care must be taken to not distort the lattice in such a way as to create weak points. Another option is to use a cylindrical cell map, this defines each unit cell based on a radial distance and an arc count (the number of unit cells at a given radius, for example in Figure 5 *b)* there are six). The downside to this approach is that the unit cells on the outer circles are likely to be significantly larger than the unit cells on the inner circles (Figure 5 *b)*).

A lattice unit cell was developed that can address the lattice fitting problem and avoid the issues that conformal and circular unit cells encounter. The new unit cell, first shown by *Atkins et al. (2019b)*,[18] uses a branching circular lattice. In this unit cell arrangement, the arc count increases with distance from the centre. The arc count is tailored so that the area covered by each unit cell, whether near the centre or the outer edge, is similar. This is shown in Figure 5 *c)*.

The primary mirror in a Cassegrain telescope requires an annulus geometry. The central part of the mirror needs to be free of any material so that redirected light can pass unobstructed. The branching circular lattice mirror requires only minor adjustments to fit an annulus base rather than a circular base. The unit cell is placed to fit exactly around the inner part of the annulus with the unit cell length designed to fit the outer circumference exactly. This is shown in Figure 5 *d)*.

3.2 Mount integration

In the original design, shown in Figure 3, the mirror mount accounts for a significant fraction of the total mirror weight. The mount is necessary to connect the mirror surface and structure to the chassis of the CubeSat. In this design the mount is a separate component from the mirror, a solid annulus with four solid spokes connecting to the corners of the CubeSat.

The concept design removed the weight of the ring by having the struts connect directly to the edge of the mirror. However, the struts were still solid and there were four struts per corner. This still represented a significant fraction of the total mirror weight. In order to maximise weight saving it was decided that the final mount should be lightweighted in a similar way as the mirror.

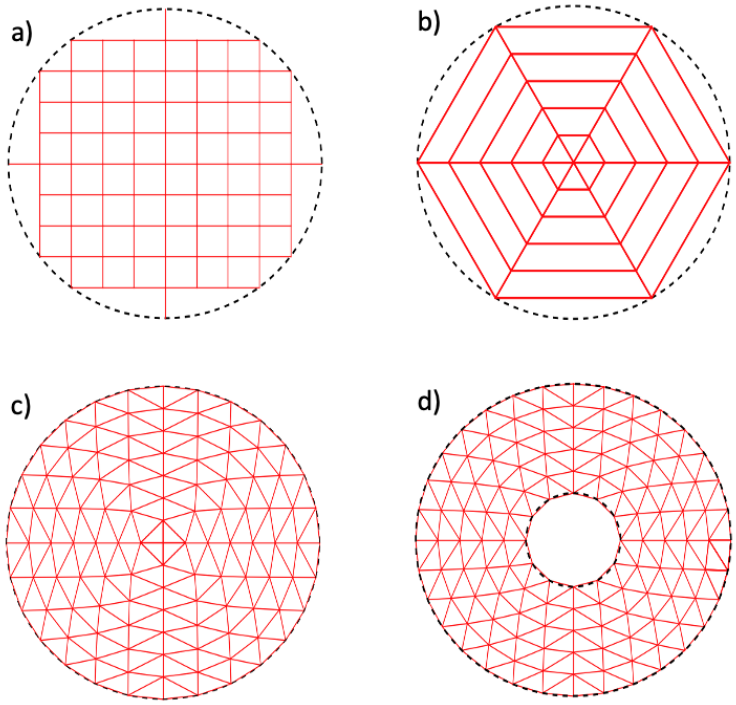

Figure 5. Distributions of unit cells within mirrors: *a)* shows a cubic unit cell and *b)* shows a cylindrical unit cell within a cylindrical mirror. The new branching circular lattice is shown in a circular geometry in *c)* and in an annulus geometry in *d)*.

The final mount design opted for a flowing curve from the outer edge of the mirror to the corners where the mirror connects to the CubeSat chassis. The curved section was selected to avoid possible stress concentrators on any sharp or irregular corners. The resultant shape, shown in Figure 6, has a much larger area than the previous strut designs. However, the component weight is still greatly reduced given the profile of the mounts and extensive use of latticing.

The distribution of the unit cells within the mount had to be modified slightly. The unit cells are still triangular prisms but did not follow the same branching circular pattern of the main mirror. Instead the triangles were distributed as evenly as possible within each mount structure. The unit cells next to the mirror were fixed to the outer cells of the mirror body, ensuring a smooth transition between the lattice in the mirror and the lattice in the mount. The unit cells on the curved edge of the mount were semi-fixed to that edge. They were free to move along the edge but not off the edge, this ensured there was no unsupported material around the edge. The remaining triangluar prisms were then adjusted until an optimal distribution of unit cells was found. The unit cell distribution in the mirror mounts is shown in Figure 6.

The method of distributing the unit cells within the body of the mirror and the mounts was kept constant throughout subsequent design iterations. The remaining design work focussed on the type of lattice in the unit cells and how the lattice interacted with the mirror surface on the top of the sandwich.

4. FIRST DESIGN ITERATION

4.1 Concept

The unit cell in the branching circular lattice is a triangular prism. In the first design iteration the lattice selected was a FCCz lattice. The 'FCC' refers to a face-centred cubic crystal structure, with the lattice nodes representing atoms and lattice struts the atomic bonds. The FCCz lattices are identical to FCC lattices but with added vertical struts. The added vertical struts improve the stiffness, especially against compressive forces.[24]

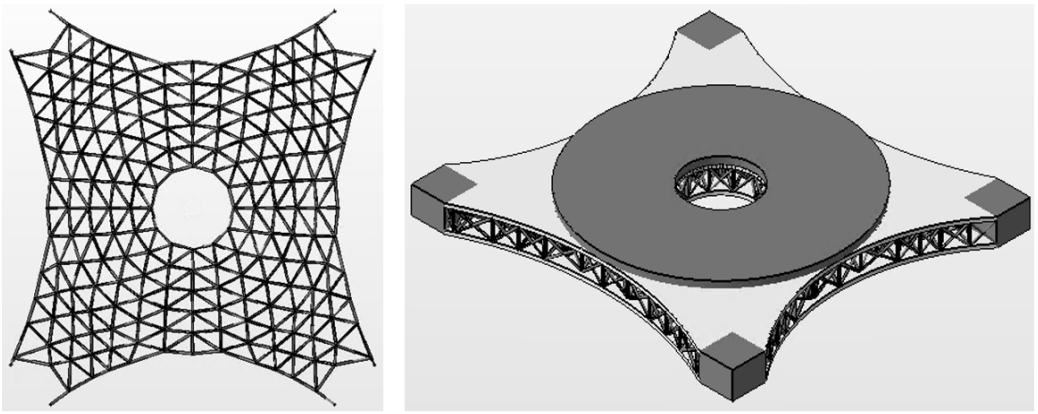

Figure 6. The integration of the mounts and latticing in the CubeSat mirror.

The original FCCz unit cell is cubic (or cuboidal) and needed modifying to fit the triangular prisms of the branching circular lattice. The modification essentially removed one of the faces from the cubic FCCz and connected the structure from either side of missing face. The lattice unit cell is shown in Figure 7. In this design not all of the the triangular prism unit cells have an equilateral triangle as the base shape. This does not affect the pattern of connecting nodes it merely distorts the angles and struts slightly for some of the unit cells.

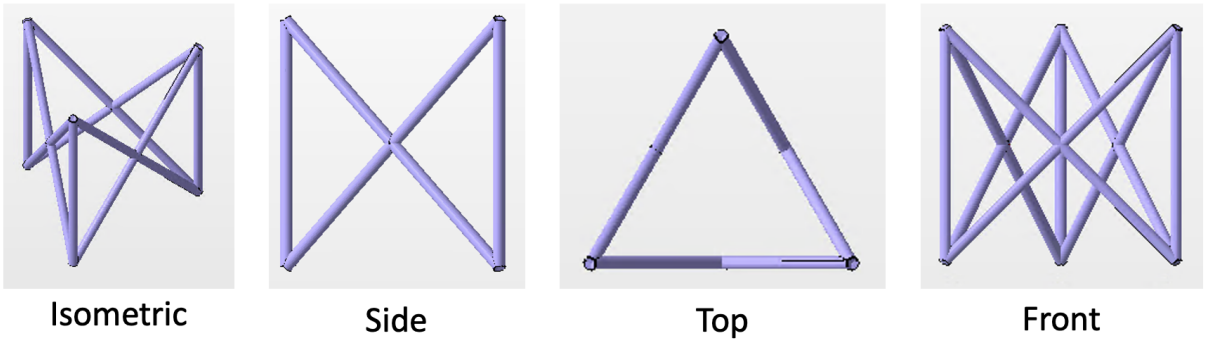

Figure 7. The FCCz lattice that has been adapted for a triangular prism unit cell.

4.2 First design review

In theory, the first design met the requirements of the mirror set out in Table 1. The dimensions had been adhered to, the mounts have been integrated and a significant fraction of weight has been saved. The optical fabrication and surface roughness are unknown without a physical part, but modelling would suggest that it is possible to achieve a good optical surface.

The design was prototyped in Ti-6Al-4V using an Arcam Q20+ electron beam melting (EBM) machine. This material and machine was selected as there is a good understanding of the build parameters and a readily available machine for rapid production. Several prototypes were build using different parameters to explore the effect on the surface quality. Examples of the titanium prototypes are shown in Figure 8 *a)* and *b)*; these prototypes were sent to the RAL Space to ensure that they could be post-processed and no design modifications for machining were required (Figure 8 *c)*).

The design requirements specify that the mirror is to be built with an aluminium alloy. The exact grade was not specified but it would likely be a high silicon aluminium alloy. To achieve this it meant it was necessary to move to a laser powder bed fusion system, as various practical limitations meant aluminium alloys could not be used on the Arcam Q20+ system.

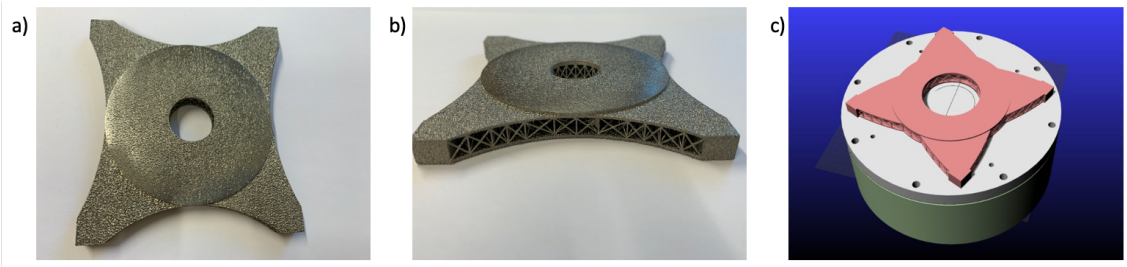

Figure 8. The first design iteration mirror. *a)* and *b)* show a prototype built in Ti-6Al-4V using EBM on an Arcam Q20+. *c)* shows a CAD representation of the design upon a single point diamond turning spindle.

Building the first design iteration on a laser system proved to be challenging. The mirror surface has a significant amount of negative space that would lead to a build failure. Negative space, also known as overhanging material, is where the material is built on top of loose powder. The loose powder acts as an insulator, in comparison to the solid material, and can lead to processing temperatures that are significantly above the intended building conditions. This can lead to many problems, including a range of defects,[25] swelling[26] and even build failures.[26]

There are three common solutions for addressing the problems with negative space. The first, and simplest, solution is changing the build orientation. Components built using AM do not have to be built in the orientation they will be used. Often building parts upside down or at some other angle will result in an easier build with less negative space. An example of this is shown in Figure 9 *a)* and *b)*.

This solution is not applicable to the first iteration design of this CubeSat mirror. The FCCz lattice builds best when the added vertical struts are kept vertical (as seen in Figure 9 *d)*). Any other angle means that some of the struts will be build at low angles and will be difficult to build. However, with the FCCz lattice the correct way up it means there is a large area of negative space on the underside of the mirror surface.

The second solution is to use a support structure. Support structures are built at the same time as the part out of the same material. Once the build is complete the support structure is then removed from the component to achieve the finished design. To aid the removal process the support structures are often designed to be purposefully weak and easy to cut or machine off. An example of this is shown in Figure 9 *c)*. Again, this solution is not applicable to the first design. The intricate and relatively close fitting lattice struts prevent supports from being removed. This is not a unique problem, support structures for inaccessible parts of components is a common design problem in AM.

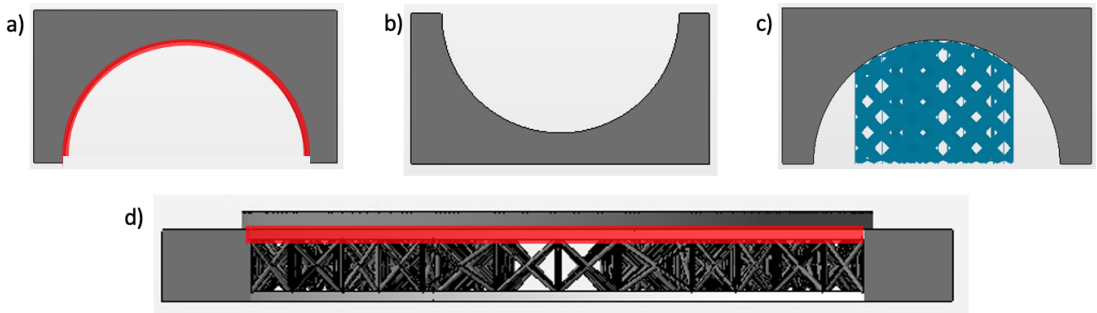

Figure 9. The negative space for an example component is shown in *a)* with the negative space is highlighted in red. The first solution, changing the build orientation, is shown in *b)*, with the negative space now removed. The second solution, adding a support structure, is shown in *c)*. The negative space in the CubeSat mirror is highlighted in red in *d)*.

The third solution, and the only viable option for this mirror design, is a redesign of the component. Modifications based on the 'printability' of the parts is a common occurrence in AM. The changes that are necessary depend on a myriad of factors, such as machine type, building technology, heat source and many other technical factors. The modifications are the main focus for the subsequent designs in the second and third iterations.

The prototypes, built using EBM, were possible as EBM is more forgiving when it comes negative space. The EBM process features a sintering stage prior to melting. The sintering stage is primarily to avoid powder disruption due to static discharges (smoke events). However, it has the added benefit that the sintered powder is better to build on than loose powder, which provides a greater tolerance of negative space.

5. FURTHER DESIGN ITERATIONS

The subsequent design iterations of mirrors directly addressed the issue of printability. Knowing that the mirrors would have to be built horizontally (i.e. with the mirror surface facing up) the designs looked to reduce negative space and provide gradual slopes to the unsupported material on the underside of the mirror surfaces. The unit cell distribution was kept the same but the lattices within the unit cells were changed.

The second design iteration was a drastic redesign of the lattice that prioritised the build angle of the lattice and supporting the mirror surface. The third design iteration remained closer to the first design concept but with an adaptation to support the mirror surface.

5.1 Second design iteration

The lattice in the second design used an hourglass shape as the inspiration, tailored to fit the the triangular prism of the branching circular lattice. The lower half has struts along the vertices of a tetrahedron (akin to a tri-pod) with a vertical strut down the middle. The top half, that connects to the mirror surface, is a solid tetrahedron, as shown in Figure 10.

The angle of the struts and the solid pyramid were set to be 45° or less (i.e. closer to vertical than horizontal). This angle was chosen as this is the maximum gradient possible on the intended AM machine. As each triangle is a slightly different size and shape it means that the angle of the lattice in each unit cell is slightly different. If the mirror was built using a different technology, with different capabilities, this angle could be adjusted. The struts were also tailored to be in the same plane as the tetrahedron faces.

Figure 10. The pyramid and lattice struts of the unit cell in the second design.

5.2 Third design iteration

The lattice in the third design used the same adapted FCCz lattice from the first design. The adaptation looked to support the mirror surface with a solid structure that sits on top of the lattice. Each unit cell has a triangle area of mirror surface that needs support. To reduce material use the mirror surface was connected to the nearest strut, on the corner of each triangle. This in effect splits each triangle up into three kite shapes, as shown in Figure 11, that are then connected to the nearest lattice strut on each corner. The angle of the kite support structure is designed to be at least 45°. The angle varies marginally with the slightly different dimensions of each triangular prism but is always at least 45°.

5.3 Overall mirror design

The two new lattices were implemented in the same distribution of unit cells throughout the mirror and mounts. A selection of 3D projections of the second and third mirror designs are shown in Figure 12 and Figure 13 respectively.

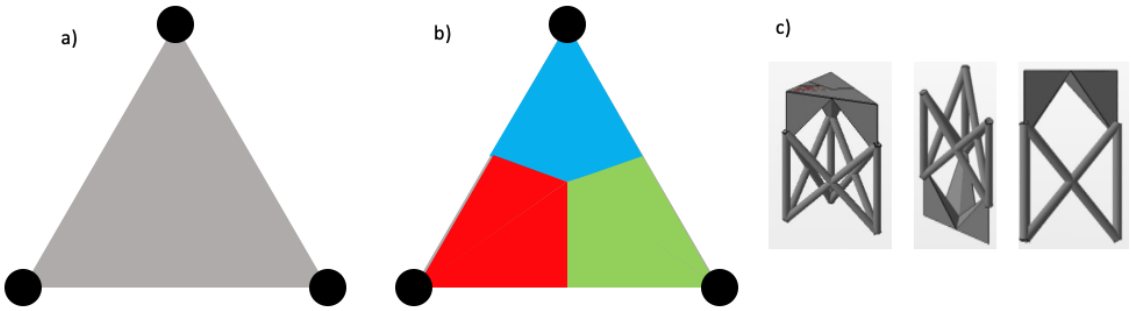

Figure 11. The kite geometries in the third iteration design. *a)* shows an example unit cell, with supports on the corner and an unsupported area in grey. *b)* shows how the triangle will be divided three regions based on the nearest lattice support. *c)* shows the end result when the unsupported area is connected to the lattice.

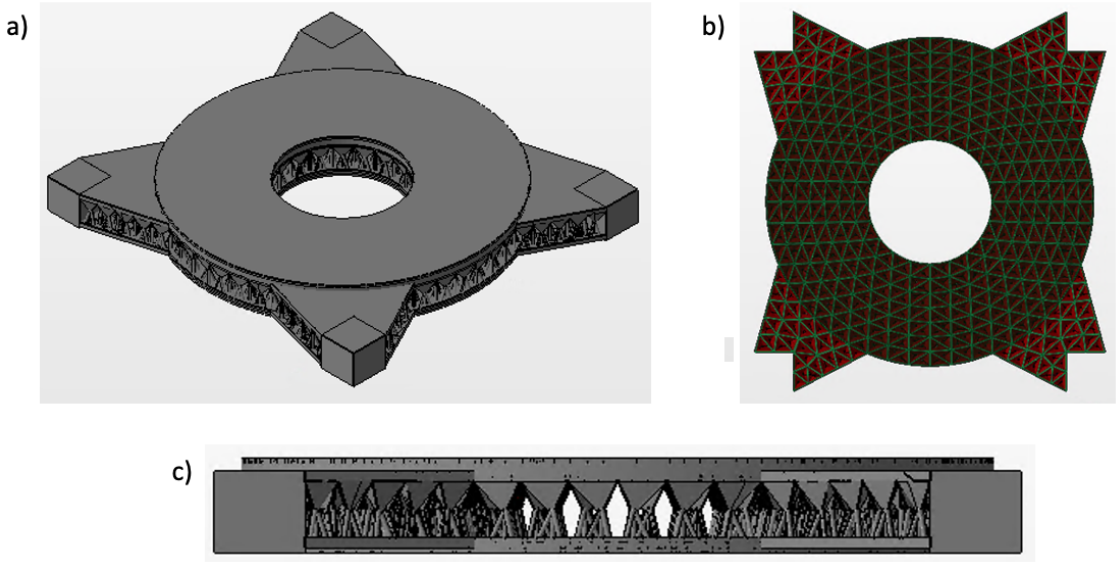

Figure 12. The second mirror design: *a)* shows a parametric view of the whole mirror. *b)* shows a cross-section just below the mirror surface. The triangle pattern of the tetrahedra match the unit cells exactly. *c)* shows a side view of the tetrahedra and supporting lattice struts.

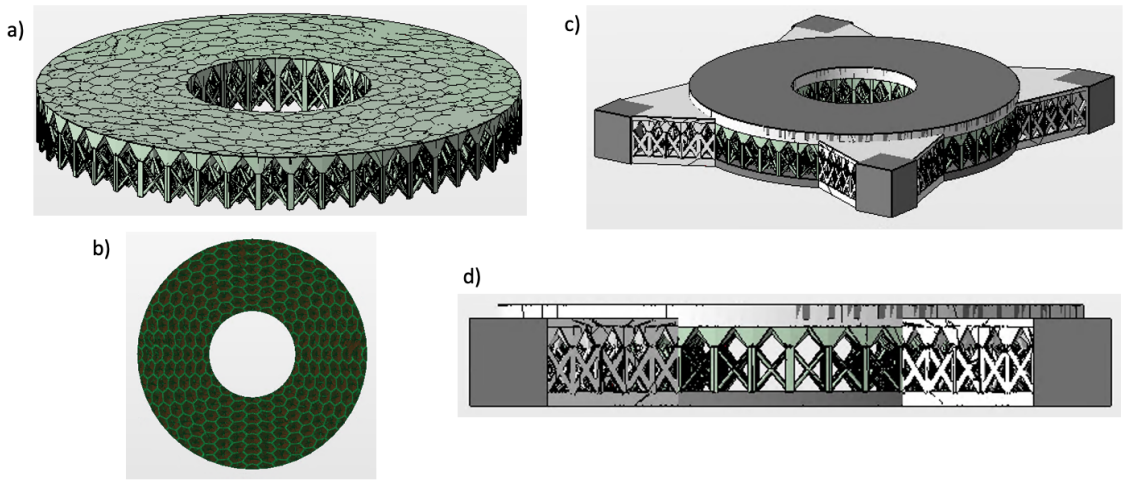

Figure 13. The third mirror design: *a)* shows the lattice without any of parts of the mirrors. *b)* shows the cross-section of the lattice part. The pattern of kites align to form hexagons around each lattice point. *c)* and *d)* shows the complete mirror from a parametric view and side view respectively.

6. FINITE ELEMENT MODEL AND ANALYSIS

The objective of the A2IM prototype was not the quality of the optical surface (form error), but rather to explore the required process chain and investigate the introduction of a conformal lattice. Therefore, FEA has been used to depict the anticipated deformations of the optical surface under a load to provide insight for future design iterations. To date, FEA has only been performed on a variant of the first design iteration (Section 4), further FEA will follow for the second and third design iterations (Section 5).

6.1 The finite element model

6.1.1 Model geometry construction and lightweighting percentage

The FEA software COMSOL Multiphysics was used for the simulations. To recreate the lattice structure, the Cartesian lattice coordinates were imported within COMSOL and connected via line profiles (Figure 14, *left*). Due to the complexity of the lattice structure, the lattice was not represented using parametric solids (cylinders), but rather as *beams*, which is an option that allows the lattice line profiles to be given a numerical thickness, but does not require them to be meshed parametric objects.[27] Table 2 provides a description of the geometrical dimensions of the prototype used within the model, as seen there is a discrepancy between the modelled values and the values within the Requirements (Table 1) this is due an earlier design variant being used in this study. Despite the geometrical differences in the design, significant deviations in FEA deformations are not expected.

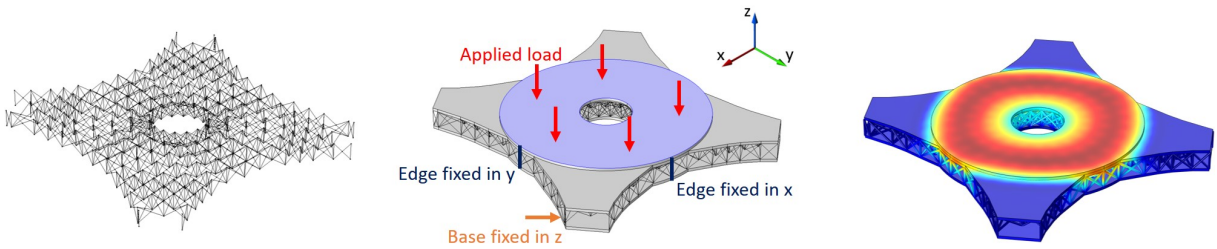

Figure 14. a) the imported lattice coordinates and generated line profiles; b) the boundary conditions applied to the model; and c) the global deformation of the of the prototype (red = maximum displacement).

The mirror lightweighting percentage was calculated numerically following Equations 1 → 4, where the length of the individual struts of the lattice, derived from the Cartesian coordinates of the strut line profiles, were summed to provide a single cylinder of length L_{latt} and radius R_{strut}. The *Solid Equivalent Vol.* is the sum of the *Plates Vol.* and the volume between the two plates. In this calculation only the mirror volume is considered, the mount is excluded. From Table 2 the mirror lightweight percentage is $\sim 37\%$ and within the original requirements.

$$Lattice\ Vol. = L_{latt}\pi R_{strut}^2 \tag{1}$$

$$L_{latt} = \sum_{n=1}^{n} \sqrt{(x_{ni} - x_{nj})^2 + (y_{ni} - y_{nj})^2 + (z_{ni} - z_{nj})^2} \tag{2}$$

$$Mirror\ Vol. = Plates\ Vol. + Lattice\ Vol. \tag{3}$$

$$Mirror\ lightweighting\ \% = \frac{Mirror\ Vol.}{Solid\ equivalent\ Vol.} \times 100 \tag{4}$$

Table 2. Geometrical dimensions of the FEA model

Property	Value
Outer diameter	72 mm⌀
Inner diameter	9 mm⌀
Mirror surface thickness	1 mm
Total height	9 mm
Lattice height	6 mm
Strut diameter	0.5 mm
Mirror lightweighting[a]	37.1 %
[a] - excluding the support structure	

6.1.2 Boundary conditions and solution extraction

The boundary conditions assume that a uniform 'polishing' load is applied to the mirror surface, the base is fixed normal to its primary surface (z-axis) and the edges along the x = 0 and y = 0 axes are fixed to allow expansion, but prevent rotation (Figure 14, *middle*). To ensure the appropriate interaction between the beams and the surface of the mirror or support, the mesh size is smaller than the strut diameter. Figure 14 *right* highlights the global distortion in terms of z-displacement of the system using these boundary conditions.

Two model variants were created, one describing the entire system (mirror and mount) and a second detailing only the mirror. The difference between the two results uncouples the effect of the integrated mount from the influence of the circular conformal lattice. It should be noted that the magnitude of the z-displacement is not the primary objective of the simulation as the exact 'polishing' pressure is unknown, rather, it is the 2-dimensional distortion profile of the FEA simulation that is of interest. Therefore, in the following section, the numerical displacements are either excluded, or normalised.

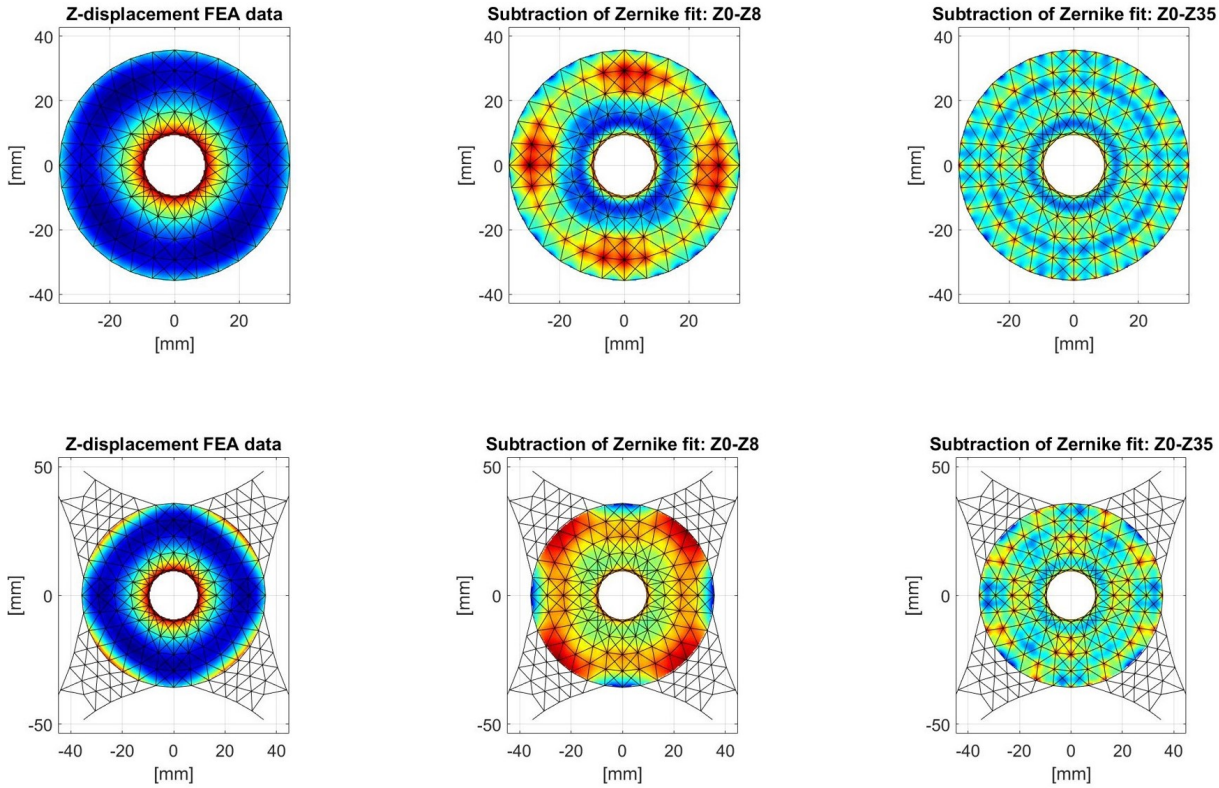

Figure 15. Analysis of the two FEA models using Zernike polynomials - mirror only (*top*), mirror and mounting (*bottom*). *Left* - the displacement normal to the optical surface from the FEA simulation; *middle* - the residual displacement data after subtraction of Zernikes Z0 - Z8; and *right* - the residual displacement data after subtraction Zernikes Z0 - Z35.

6.2 Zernike analysis

To explore how the FEA distortion propagate into optical distortions observed with an interferometer, the FEA distortion maps (z-displacement) were analysed using circular Zernike polynomials from Z0 - Z35.[28] The Zernike polynomials were mapped onto the FEA data using MATLAB and least squares fitting was used to calculate the magnitude of each term. Figure 15 highlights graphically the FEA data after the subtraction of Zernike terms Z0-Z8 (*middle*) and Z0-Z35 (*right*) for the mirror only (*top*) and the mirror and support (*bottom*).

Figure 16 presents the normalised magnitudes of each of the Zernike coefficients for the two cases. The dominant term in both cases is spherical defocus (Z8). In the mirror only case, the dominant terms are spherical (Z3, Z8, Z15, Z24 & Z35) with minor contributions from tetrafoil terms (Z16 & Z27). Whereas, for the case of the mirror and mounting, after the dominant contribution from spherical defocus, the spherical and tetrafoil terms have similar weighting. In both models the presence of tetrafoil is expected: in the mirror and mounting model, the four arms of the integrated support are observed within the mirror surface (Figure 15 *bottom* - *middle*); and in the mirror only model, a non uniformity of the lattice structure has resulted in four over supported regions on the mirror surface (Figure 15 *top* - *middle*) - this non uniform lattice structure was subsequently removed in the final version of the first design iteration (Section 4). The difference in the direction of the tetrafoil (Z16) in both cases is shown by the change of sign in Figure 16.

As shown in both models, low order distortions dominate the mirror surface and it is only on the removal of the first 36 Zernike terms that the print-through effect of the struts is prominent. Although an FEA simulation is not a perfect prediction of the outcome of optical post-processing, it does provide an indication as demonstrated in *Atkins, et al. (2019)*[17]. The FEA - Zernike analysis can be used as a means to optimise the lattice structure in order to minimise the spherical and tetrafoil deformations. There are several methods that can be employed to achieve this, such as increasing or decreasing the thickness of certain rings of struts, or re-positioning the

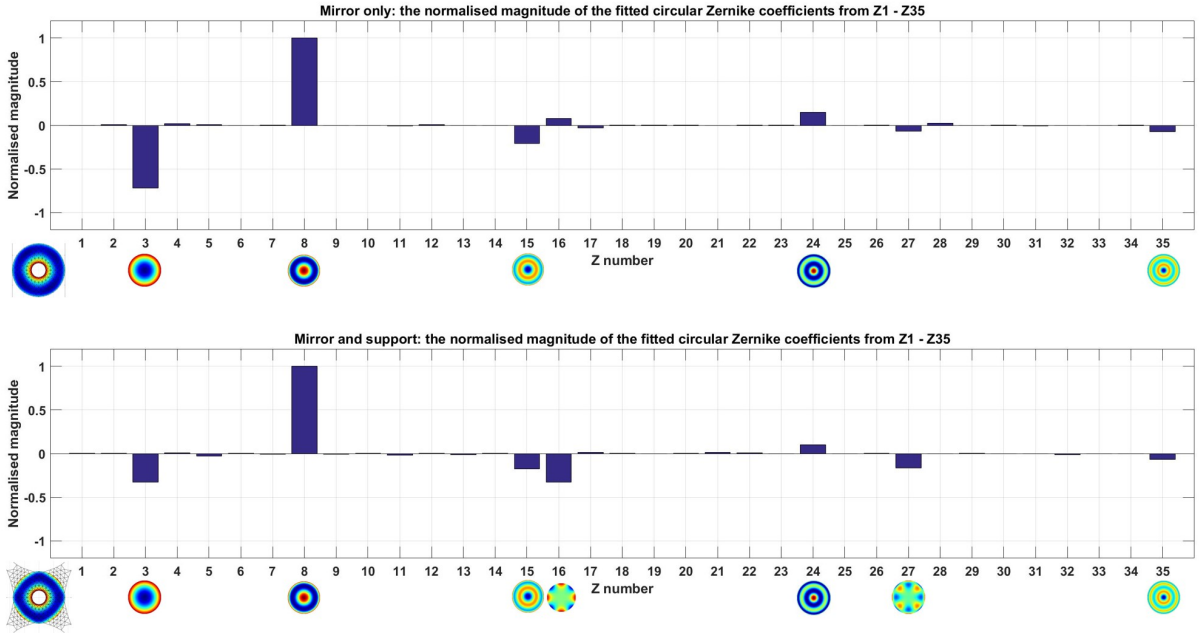

Figure 16. The normalised magnitude of the individual Zernike terms (Z1 $\longrightarrow$ Z35) for the mirror only model (*top*) and the mirror and mount model (*bottom*).

azimuthal rings of the lattice to preferential radial locations[18] as determined by TO. To reduce the tetrafoil, a less direct connection from the optical surface to the mounting structure can be considered - i.e. isolating the mirror surface from the mounting surface but maintaining the lattice connection.

7. SUMMARY AND FUTURE WORK

This work looked to develop a lightweight CubeSat mirror through part integration and utilisation of non-standard lattices. In this regards, the work so far has been successful although incomplete. All three designs have incorporated mounts and have lattices that provide support while avoiding the geometry challenges observed in conventional open-back or sandwich lightweight mirrors. The objective of this work was the exploitation of the AM design space while simultaneously ensuring that the design could be printed and post-processed.

The first design iteration used an adaptation of a FCCz lattice. The structure was lightweight and stiff but was difficult to build using laser powder bed fusion AM systems. The FEA highlighted that the anticipated dominant form errors would be spherical for the mirror only and spherical and tetrafoil for the mirror and mount. Future design optimisations can utilise the FEA information to minimise these effects and then refocus efforts on minimising the print-through of the lattice struts. Ray tracing software, such as Zemax, can be employed to estimate how the print-through surface deformations affect the optical performance of the system.

The second and third iterations were designed to accommodate the limitations of printing using a laser powder bed fusion system. Angled structures provided a transition between the mirror surface and the lightweight lattice structure. This will make the mirrors printable using a laser system and to allow progress with the experimental prototyping phase of the study. It is anticipated that in the first quarter of 2021 that the second and third iterations will be built and that conventional machining, SPDT and an analysis of the optical surface will follow.

Further FEA will be performed on the second and third designs and it is anticipated that the print-through effect of the lattice struts will be reduced due to the additional tetrahedral support added to the lattice. However, this additional support will add weight to the system and it is so far undetermined whether this additional material will cause the mirror to exceed the desired lightweighting percentage noted in the requirements.

ACKNOWLEDGMENTS

This project has received funding from the European Union's Horizon 2020 research and innovation programme under grant agreement No 730890. This material reflects only the authors views and the Commission is not liable for any use that may be made of the information contained therein.

The authors acknowledge MAPP: EPSRC Future Manufacturing Hub in Manufacture using Advanced Powder Processes (EP/P006566/1) and the Sir Henry Royce Institute for access to the Arcam Q20+ (EP/P02470X/1).

REFERENCES

[1] Schnetler, H., Atkins, C., Miller, C., Morris, K., Hugot, E., Roulet, M., Tenegi, F., Vega-Moreno, A., Farkas, S., Mező, G., Snell, R. M., Dufils, J., and van de Vorst, B., "H2020 opticon project overview: Investigating the use of additive manufacturing for the design and build of multi-functional integrated astronomical components," *Proc. of SPIE* **11451**, SPIE Astronomical Telescopes + Instrumentation (2020).

[2] Farkas, S., Agócs, T., Atkins, C., Bouwers, L., Dufils, J., Joó, A., Mező, G., Morris, K., Rodenhuis, M., Roulet, M., Schnetler, H., Snell, R., Tenegi, F., Vega-Moreno, A., and van de Vorst, B., "Freeform active mirror designed for additive manufacturing," *Proc. of SPIE* **11451**, SPIE Astronomical Telescopes + Instrumentation (2020).

[3] Vega, A., Tenegi, F., Márquez-Rodríguez, J. F., van de Vorst, B., Dufils, J., Brouwers, L., Snell, R. M., Schnetler, H., Atkins, C., Miller, C., Morris, K., Roulet, M., Hugot, E., Farkas, S., and Mező, G., "Design for Additive Manufacturing (DfAM): The 'Equivalent Continuum Material' for cellular structure analysis," *Proc. of SPIE* **11451**, SPIE Astronomical Telescopes + Instrumentation (2020).

[4] Roulet, M., Atkins, C., Hugot, E., Snell, R., van de Vorst, B., Morris, K., Marcos, M., Todd, I., Miller, C., Dufils, J., Farkas, S., Mezo, G., Tenegi, F., Vega-Moreno, A., and Schnelter, H., "Use of 3D printing in astronomical mirror fabrication," in [*3D Printed Optics and Additive Photonic Manufacturing II*], **11349**, International Society for Optics and Photonics, SPIE (2020).

[5] Herzog, H., Segal, J., Smith, J., Bates, R., Calis, J., De La Torre, A., Kim, D. W., Mici, J., Mireles, J., Stubbs, D. M., and Wicker, R., "Optical fabrication of lightweighted 3d printed mirrors," *Proc. SPIE* **9573**, 957308–957308–15 (2015).

[6] Sweeney, M., Acreman, M., Vettese, T., Myatt, R., and Thompson, M., "Application and testing of additive manufacturing for mirrors and precision structures," *Proc. SPIE* **9574**, 957406–957406–13 (2015).

[7] Atkins, C., Feldman, C., Brooks, D., Watson, S., Cochrane, W., Roulet, M., Hugot, E., Beardsley, B., Harris, M., Spindloe, C., Alcock, S. G., Nistea, I.-T., Morawe, C., and Perrin, F., "Topological design of lightweight additively manufactured mirrors for space," *Proc. of SPIE* **10706** (2018).

[8] Tan, S., Ding, Y., Xu, Y., and Shi, L., "Design and fabrication of additively manufactured aluminum mirrors," *Optical Engineering* **59**(1), 1 – 17 (2020).

[9] Woodard, K. S. and Myrick, B. H., "Progress on high-performance rapid prototype aluminum mirrors," in [*Advanced Optics for Defense Applications: UV through LWIR II*], Vizgaitis, J. N., Andresen, B. F., Marasco, P. L., Sanghera, J. S., and Snyder, M. P., eds., **10181**, 177 – 182, International Society for Optics and Photonics, SPIE (2017).

[10] Hilpert, E., Hartung, J., Risse, S., Eberhardt, R., and Tünnermann, A., "Precision manufacturing of a lightweight mirror body made by selective laser melting," *Precision Engineering* **0141-6359** (2018).

[11] Hilpert, E., Hartung, J., von Lukowicz, H., Herffurth, T., and Heidler, N., "Design, additive manufacturing, processing, and characterization of metal mirror made of aluminum silicon alloy for space applications," *Optical Engineering* **58**(9) (2019).

[12] Heidler, N., Hilpert, E., Hartung, J., von Lukowicz, H., Damm, C., Peschel, T., and Risse, S., "Additive manufacturing of metal mirrors for TMA telescope," in [*Optical Fabrication, Testing, and Metrology VI*], Schröder, S. and Geyl, R., eds., **10692**, 92 – 98, International Society for Optics and Photonics, SPIE (2018).

[13] Mici, J., Rothenberg, B., Brisson, E., Wicks, S., and Stubbs, D. M., "Optomechanical performance of 3d-printed mirrors with embedded cooling channels and substructures," *Proc.SPIE* **9573**, 9573 – 9573 – 14 (2015).

[14] Hu, R., Chen, W., Li, Q., Liu, S., Zhou, P., Dong, Z., and Kang, R., "Design optimization method for additive manufacturing of the primary mirror of a large-aperture space telescope," *Journal of Aerospace Engineering* **30**(3), 04016093 (2017).

[15] Liu, J. and Jiang, B., "Topology optimization design of a space mirror," *Proc. SPIE* **9795**, 97952Y–97952Y–10 (2015).

[16] Qu, Y., Wang, W., Liu, B., and Li, X., "Topology optimization design of space rectangular mirror," *Proc. SPIE* **10154**, 1015421–1015421–7 (2016).

[17] Atkins, C., Brzozowski, W., Dobson, N., Milanova, M., Todd, S., Pearson, D., Brooks, D., Bourgenot, C., Snell, R. M., Sun, W., Cooper, P., Alcock, S. G., and Nistea, I.-T., "Additively manufactured mirrors for cubesats," *Proc. of SPIE* **11116-41** (2019).

[18] Atkins, C., Brzozowski, W., Dobson, N., Milanova, M., Todd, S., Pearson, D., Brooks, D., Bourgenot, C., Snell, R. M., Sun, W., Cooper, P., Alcock, S. G., and Nistea, I.-T., "Lightweighting design optimisation for additively manufactured mirrors," *Proc. of SPIE* **11116-42** (2019).

[19] Vukobratovich, D., [*Optomechanical Engineering Handbook - Chapter 5: Lightweight Mirror Design*], CRC Press LLC (1999).

[20] Allthorpe-Mullis, E., Brzozowski, W., Easdown, W., Feore, D., Grainger, W., Greenland, S., Hodgkins, M., Milanova, M., Payne, S., Pearson, D., Rowan, C., and Todd, S., "Cubesat camera: A low cost imaging system for cubesat platforms," **Proceedings of iCubeSat 2018** (2018).

[21] Montagnino, L. A., "Test And Evaluation Of The Hubble Space Telescope 2.4-meter Primary Mirror," in [*Large Optics Technology*], **0571**, 182 – 190, International Society for Optics and Photonics, SPIE (1986).

[22] Deppo, V. D., Pace, E., Morgante, G., Focardi, M., Terraneo, M., Zocchi, F., Bianucci, G., and Micela, G., "A prototype for the primary mirror of the ESA ARIEL mission: design and development of an off-axis 1-m diameter aluminum mirror for infrared space applications," in [*Advances in Optical and Mechanical Technologies for Telescopes and Instrumentation III*], **10706**, 901 – 911, International Society for Optics and Photonics, SPIE (2018).

[23] Martin, H. M., "Making mirrors for giant telescopes," in [*Astronomical Optics: Design, Manufacture, and Test of Space and Ground Systems II*], **11116**, 150 – 165, International Society for Optics and Photonics, SPIE (2019).

[24] Maconachie, T., Leary, M., Lozanovski, B., Zhang, X., Qian, M., Faruque, O., and Brandt, M., "Slm lattice structures: Properties, performance, applications and challenges," *Materials & Design* **183**, 108137 (2019).

[25] Snell, R., Tammas-Williams, S., Chechik, L., Lyle, A., Hernández-Nava, E., Boig, C., Panoutsos, G., and Todd, I., "Methods for rapid pore classification in metal additive manufacturing," *JOM* **72**(1), 101–109 (2020).

[26] Boone, N., *Near Infrared Thermal Imaging for Process Monitoring in Additive Manufacturing*, PhD thesis, University of Sheffield (June 2020).

[27] COMSOL Multiphysics, "Pratt truss bridge v5.5." https://uk.comsol.com/model/pratt-truss-bridge-8511 (2019).

[28] Goodwin, E. P. and Wyant, J. C., [*Field Guide to Interferometric Optical Testing*], SPIE Press (2006).